Real Time Visualization of Active Species in a Single-Site Metal-Organic Framework Photocatalyst

Sizhuo Yang, a‡ Brian Pattengale, a‡ Sungsik Lee, b Jier Huang a*

^aDepartment of Chemistry, Marquette University, Milwaukee, Wisconsin, 53201

^bX-ray Science Division, Argonne National Laboratory, Argonne, Illinois, 60349

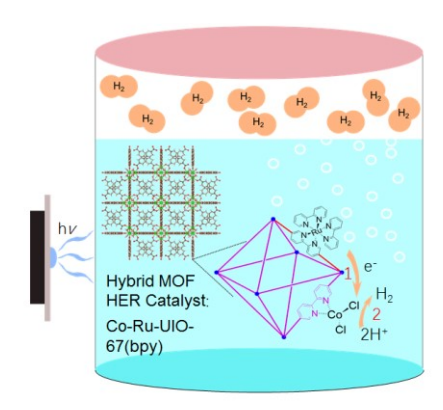
AUTHOR INFORMATION

Corresponding Author

*Jier Huang (jier.huang@marquette.edu)

ABSTRACT In this work, we report a new single-site photocatalyst (Co-Ru-UIO-67(bpy)) based on metal organic framework platform with incorporated molecular photosensitizer and catalyst. We show that this catalyst not only demonstrates exceptional activity for light-driven H₂ production but also can be recycled without loss of activity. Using the combination of optical transient absorption (OTA) spectroscopy and *In Situ* X-ray absorption spectroscopy (XAS), we not only captured the key Co^I intermediate species formed after ultrafast charge transfer from the incorporated photosensitizer but also identified the rate limiting step in catalytic cycle, providing insight into the catalysis mechanism of these single-site metal-organic framework photocatalysts.

TOC GRAPHICS



The direct conversion of solar energy to clean fuel as alternatives to fossil fuels is a desirable approach to address the global energy and environmental problems.¹⁻⁵ Hydrogen generation through water splitting is an emerging strategy of doing so that has attracted great attention, yet its development is largely hampered by the difficulty in efficient integration of multiple resource-intensive processes, i.e. light absorption, charge separation, and finally utilization of the photogenerated carriers to drive water splitting. Homogeneous solution based systems comprising of molecular photosensitizer (PS) and catalysts have naturally attracted much attention due to their merit in synthetic control over functional tunability and selectivity.⁶⁻¹⁰ However, their limited stability and efficiency remains a major challenge. In contrast, heterogeneous systems have shown beneficial features in long-term durability and high catalytic activity.¹¹⁻¹³ However, these materials not only lack design flexibility but also suffer from the difficulty in characterizing their mechanistic functions, rendering poor understanding of the origins behind their remarkable catalytic efficiency.

Due to their unique capability in combining the most advantageous features of heterogeneous and homogeneous catalysts, metal organic frameworks (MOFs) are one of the best solutions to the above-mentioned stability and efficiency issues. 14-18 MOFs have the ability to incorporate homogeneous catalytic components in their heterogeneous matrix to achieve isolated active sites. 19-23 As such, MOFs can offer the same level of advantages as homogeneous catalysts while the robustness of the catalysts are increased. In addition, MOFs are built from periodic organic bridging ligands and inorganic nodes with tunable pore structure and functional components, which not only allows precise determination of the nature of the incorporated catalytic active sites, but also opens up the possibility to engineer MOF catalytic sites in a defined manner. 24-26

Due to these reasons, an increasing number of systems that demonstrate successful application of MOFs in photocatalysis, with either a molecular PS or a molecular catalyst incorporated in the structure, have emerged. For example, photosensitizers such as porphyrin, ²⁶⁻³⁰ Ru complexes, ³¹⁻³⁴ and tetraphenylethylene, ³⁵ etc. have been successfully incorporated into MOFs for their beneficial photophysical properties. Meanwhile, molecular catalysts based on Ru, ³⁶ Re, ³⁷⁻³⁸ Ir, ^{22, 37} Co, ^{19, 21, 39} Fe, ⁴⁰⁻⁴¹ Rh, ^{20, 42} Pt, ^{34, 43-44} Pd, ⁴⁵ have been introduced into MOF structure and demonstrated catalytic activities. Despite these progresses, there are only two examples that reported the immobilization of both molecular photosensitizers (RuDCBPY, ³⁴ Ir(III)DCBPY⁴³) and molecular catalysts (PtDCBPY) into the framework structure, both of which indeed showed enhanced activities for H₂ generation compared to their corresponding homogeneous counterpart. Offering their large potential as efficient photocatalytic systems for solar fuel conversion as well as the ease for fundamental studies of MOF structure/catalytic function relationships, such single solid platform are especially ripe targets for further development.

In this work, we report a new single site MOF system that incorporates a molecular catalyst based on earth-abundant metal and Ru based PS to UIO-67(bpy), which not only demonstrates exceptional catalytic activities, but also is recyclable and reusable for H₂ evolution reaction (HER). More importantly, we established the fundamental structure-function relationships of this system for HER examined under standard catalytic conditions. Using *in situ* X-ray absorption spectroscopy, we identified the intermediate species that determines the rate limiting step and unravel the origins of induction period, a complication that has long plagued mechanistic investigations in catalysis. Using time-resolved absorption spectroscopy, we elucidated the

fundamental origins of light harvesting and charge transfer dynamics, the properties that essentially dictate the function of this system for photocatalysis.

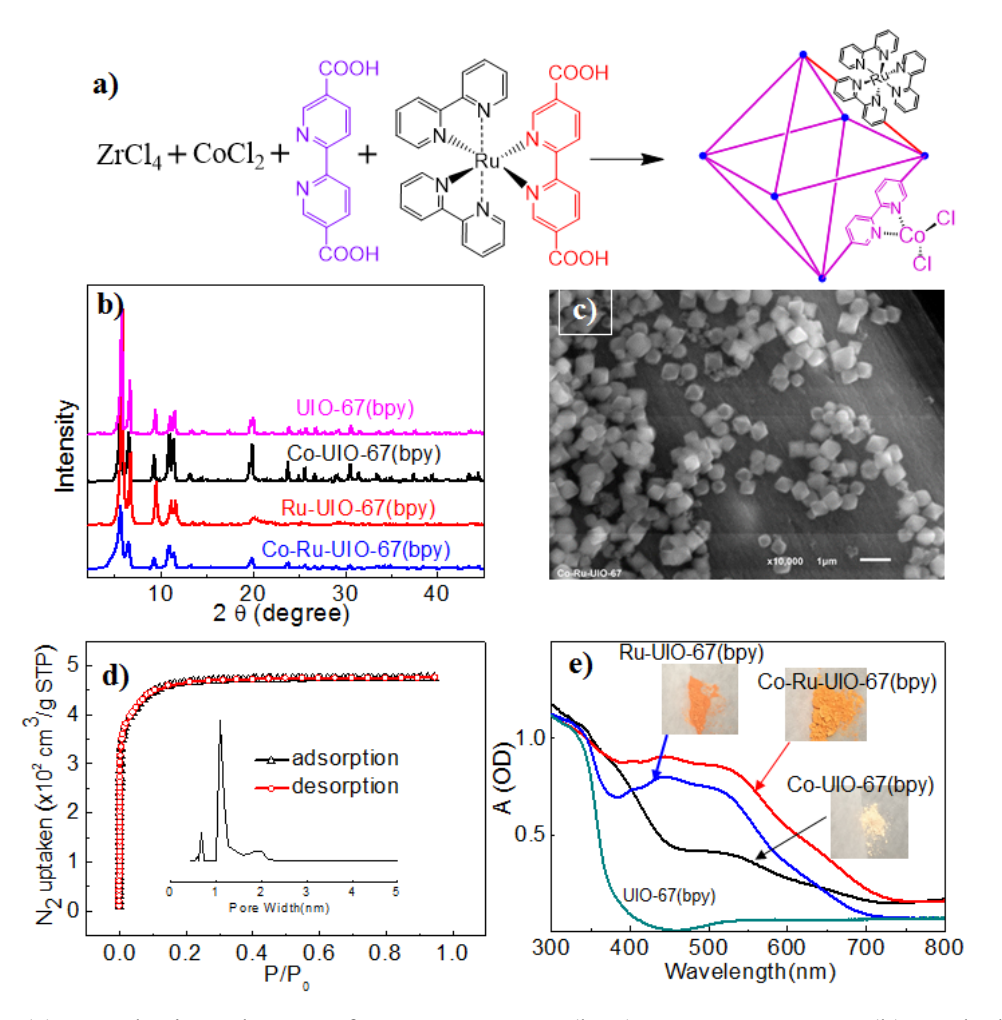


Figure 1. (a) Synthetic scheme of Co-Ru-UIO-67(bpy). XRD patterns (b) and diffuse reflectance spectra (e) for UIO-67(bpy), Co-UIO(bpy), Ru-UIO(bpy), and Co-Ru-UIO(bpy). (c) SEM image of Co-Ru-UIO-67(bpy). (d) N₂ adsorption isotherm and pore size distribution (inset) of Co-Ru-UIO-67(bpy).

As shown in Figure 1a, Co-Ru-UIO-67(bpy) was synthesized according to previous published protocols⁴⁶⁻⁴⁷ by mixing ZrCl₄ (50.0 mg, 0.21 mmol), 2,2-bipyridine-5,5-dicarboxylic acid (H₂bpdcy) (45.0 mg, 0.19 mmol), Rudcbpy ([Ru(dcbpy)(bpy)₂] Cl₂, 10.0 mg, 0.012 mmol), CoCl₂(25.0mg, 0.19mmol) and glacial acetic acid (93 μL, 1.6 mmol) in DMF (20 mL). Rudcbpy

was prepared according to the previously published method.⁴⁸ As controls, UIO-67(bpy), Ru-UIO-67(bpy) and Co-UIO-67(bpy) were also synthesized under the similar conditions.

The XRD patterns of these MOFs (Figure 1b) agree well with the patterns for UIO-67, suggesting that the crystallinity of these MOFs retain after incorporation of molecular complexes. 49 SEM image of Co-Ru-UIO-67(bpy) (Figure 1c) shows that the sample exhibits an octahedral crystalline structure with particle size ~ 500 nm. The porous structure of Co-Ru-UIO-67(bpy) was confirmed by BET analysis. As shown in Figure 1d, the surface area and pore size of Co-Ru-UIO-67(bpy) are 1781 m²/g and 1.65 nm, respectively, which are close to those of UIO-67(bpy) (Figure S1) and comparable to literature data.⁵⁰ The presence of Ru and Co complexes was supported by diffuse reflectance UV-visible spectroscopy. As shown in Figure 1e, the additional broad absorption in the range of 350-700 nm in Co-Ru-UIO-67(bpy) compared to that of UIO-67(bpy) is consistent with the absorption features of Co complex in Co-UIO-67(bpy) and Ru complexes in Ru-UIO-67(bpy), and thus can be attributed to the absorption resulting from Co- and Ru-complexes incorporated into UIO-67(bpy). The concentrations of Co measured by inductively coupled plasma mass spectrometry (ICP-MS) and Ru measured by atomic absorption spectroscopy in Co-Ru-UIO-67(bpy) are 5.68 x 10⁻⁷ mol/mg and 1.08 x 10⁻⁷ mol/mg, respectively, corresponding to the elemental ratio of Co:Ru =5.26.

The direct incorporation of Co complex into UIO-67(bpy) structure as well as its local structure at Co center was confirmed by steady-state X-ray absorption spectroscopy (XAS) measured at Advanced Photon Source, Argonne National Laboratory. Figure 2a compares X-ray absorption near edge structure (XANES) spectra for Co-UIO-67(bpy) and Co-Ru-UIO-67(bpy) at Co K-edge. The XANES spectra of two reference samples with different geometry, i.e. the distorted tetrahedral Co complex (Co(6,6'-Dimethyl-2,2'-bipyridine)Cl₂, abbreviated as

Co(dmbpy)Cl₂) and CoO (octahedrally coordinated Co center), are also shown in Figure 2a in order to correlate the spectral shape with local structure. The spectrum of Co(dmbpy)Cl₂ is featured by a prominent pre-edge feature corresponding to the dipole forbidden 1s-3d transition (inset of Figure 2a), supporting the non-centrosymmetric geometry about Co due to distorted

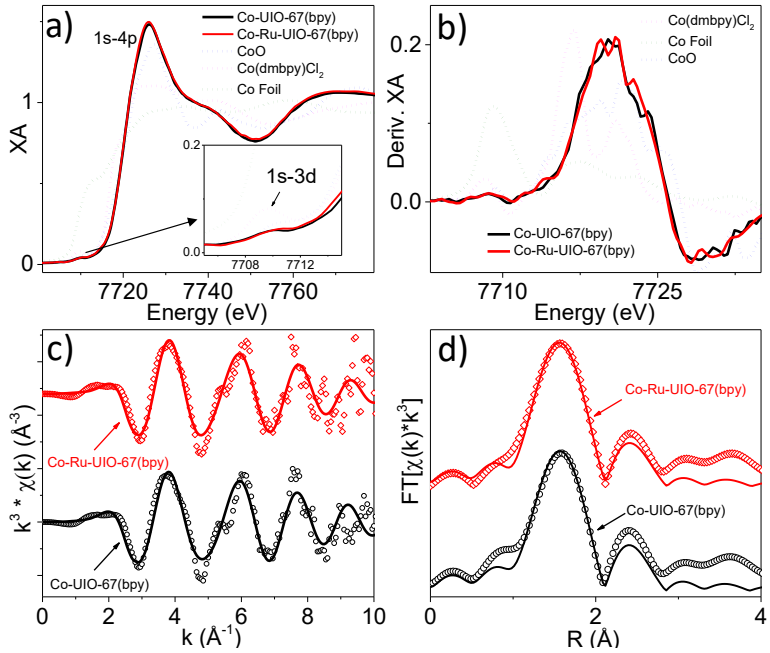


Figure 2. The Co K-edge XANES spectra of Co-UIO-67(bpy) and Co-Ru-UO-67(bpy) samples (solid lines) and Co^{II}, Co⁰ reference compounds (dotted lines) (a) and their first derivative spectra (b). The K-space (c) and Fourier-transformed R-space (d) spectra compared with data as open points and FEFF fits as solid lines. Inset of (a) shows enlarged pre-edge feature.

tetrahedral structure.⁵¹ In contrast, the XANES spectrum of octahedral CoO presents relatively weak pre-edge feature due to centrosymmetric geometry at Co center.⁵²⁻⁵³ Both Co-UIO-67(bpy) and Co-Ru-UIO-67(bpy), which have nearly identical XANES spectra to one another, show similar XANES features as that of CoO, suggesting that Co centers in both samples likely possess octahedral geometry. Moreover, the edge energy of the XANES spectra of both MOF samples, as shown in the first derivative XANES spectra (Figure 2b), show excellent agreement

with the edge position of CoO reference, suggesting that Co centers in MOF samples retain +2 oxidation state.

The local geometry of Co^{II} center in Co-UIO-67(bpy) and Co-Ru-UIO-67(bpy) samples, revealed by XANES studies above, indicates that Co is coordinated by more than four atoms, implying that solvents may have participated in coordination to Co center in the Co(bpy)Cl₂ moiety. This assignment is further supported by a recent literature report,⁵⁴ where single-crystal X-ray diffraction data confirmed the presence of 5 and 6-coordinated Co sites in a Zr-based MOF with CoCl₂ metalation of its bipyridine linkers due to coordination of Co to either one or two solvent molecules. In order to quantitatively support this assignment, the full EXAFS energy range spectra (Figure S2) were fit using the Demeter X-ray absorption analysis package.⁵⁵ The FEFF input model was built from the crystal structure of Co(dmbpy)Cl₂ by adding an additional solvent molecule (methanol) coordinated to Co. The scattering amplitude of the Co-solvent single scattering vector in the first shell of atoms about Co was parameterized to allow its variation with the other fitting parameters and was interpreted as the average solvent coordination number. The details of EXAFS fitting are discussed in SI with fitting parameters listed in Table S1 and a graphic of the fitting model in Figure S2. The EXAFS data and the resulting best fits in K-space and R-space are shown in Figure 2c and Figure 2d, respectively. From the best fitting results, the bond distance of Co to N atoms on bipyridine in Co-UIO-67(bpy) and Co-Ru-UIO-67(bpy) is determined to be 2.08 Å and 2.09 Å, respectively, and the Co-Cl distance for both samples is 2.29 Å. The Co to solvent atom distance is 1.92 Å with coordination number of approximately 1.1 for both samples. The Co-N distances are within the range of distances reported in the literature (2.09 and 2.17 for 5-coordinate Co; 2.01 and 2.13 for 6-coordiate Co), as are the Co-Cl distances (2.27 and 2.31 for 5-coordinate Co; 2.27 and 2.33 for

6-coordinate Co),⁵⁴ suggesting the validity of our fitting model. With these insights into the structure/properties of Co-Ru-UIO-67(bpy), in the following sections, we investigate its catalysis activity for HER and fundamentally characterize its catalytic mechanism.

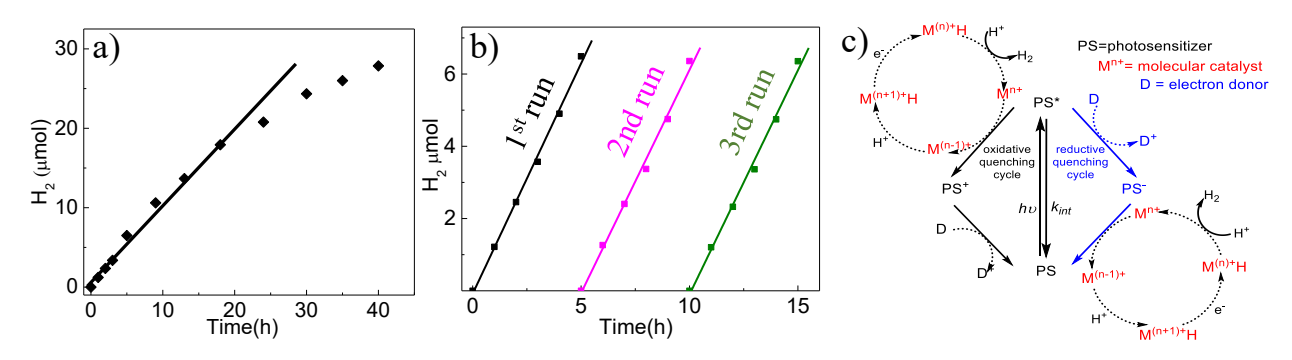


Figure 3. (a) Time profile of H₂ production by Co-Ru-UIO-67(bpy) under 447 nm LED illumination at 9 mW in the presence of TEOA (0.3 mL) and H₂O (0.4 mL) in acetonitrile solution (3 mL). (b) Recycling of Co-Ru-UIO-67(bpy) catalyst after multiple 5-hour experiments. (c) Commonly accepted catalytic pathway for photoinduced H₂ generation with molecular photosensitizer (PS) and catalysts.

The photocatalytic performance of Co-Ru-UIO-67(bpy) for HER was tested under the illumination of a 447 nm LED lamp in the mixture of H₂O and acetonitrile solution. The reaction conditions, including sacrificial donors, the concentrations of sacrificial donors and MOFs, proton sources, the ratios of catalyst to PS, and LED powers were systematically optimized to reach the maximum amount of H₂ per gram of catalyst (Figure S3). The optimized conditions for the Co-Ru-UIO-67(bpy) photocatalytic system is under Co:Ru = 5.26:1 of Co-Ru-UIO-67(bpy) (1.0 mg), 0.4 mL of H₂O, and 0.3 mL of TEOA, and 9 mW LED power in 3 mL acetonitrile solution. Control experiments omitting TEOA or H₂O did not yield H₂, suggesting their key roles as sacrificial donor and proton source (Figure S4). For comparison, Co-UIO-67(bpy) or Ru-UIO-67(bpy) with the same metal loading as that in Co-Ru-UIO-67(bpy) only yields minimal amount of H₂ under identical conditions (Figure S4), indicating incorporating both Ru PS and Co catalysts into the MOF structure is essential for HER. Under these

conditions, the HER activity of Co-Ru-UIO-67(bpy) achieves 27,853 mol H₂/g of MOF after 40 hours (Figure 3a), which accounts for TON of 99 based on Co and is comparable to previous MOF systems containing Pt complexes as catalysts.^{34, 56} The current system, however, benefits from the use of earth abundant Co complex as catalysts.

To evaluate the duration of the Co-Ru-UIO-67(bpy) catalytic system, the recycling tests were explored by collecting MOFs after each 5 hours' illumination via centrifugation and dispersal in a fresh catalysis solution. Remarkably, Co-Ru-UIO-67(bpy) shows unchanged activity during the recycling experiments for at least three runs. Furthermore, the concentration of Co in the supernatant solution before and after catalysis was measured using ICP-MS to examine the possibility of Co leaching. While ~ 3.2% of Co is leached during catalysis process, HER experiments using supernatant solution under the same conditions did not yield detectable amount of H₂, ruling out the possibility that the observed activity is due to leached Co. To further confirm the integrity of the MOF photocatalyst after catalysis, ex situ XAS was performed in which the MOF photocatalyst was removed from the catalysis solution after 20 hours and washed via centrifugation. The XANES and EXAFS results (Figure S5 and Table S2) indicate that the local structure of Co remains unchanged after catalysis. The significantly improved activity and stability suggest the important role of the framework in both boosting the catalytic activity of molecular catalysts and stabilizing the catalytic species, which prompted us to investigate the mechanistic origins of its catalytic function.

As shown in Figure 3c, a commonly accepted scheme for photoinduced proton reduction is initiated with light absorption by PS, which is followed by two sequential charge separation (CS) processes, where the electrons in the excited PS transfer to the catalyst and holes are extracted to electron donors through either the reductive or oxidative cycle. Consequently, it is crucial to have a systematic study of these light harvesting and CS dynamics in Co-Ru-UIO-67(bpy) to gain mechanistic insight of its function for catalysis.

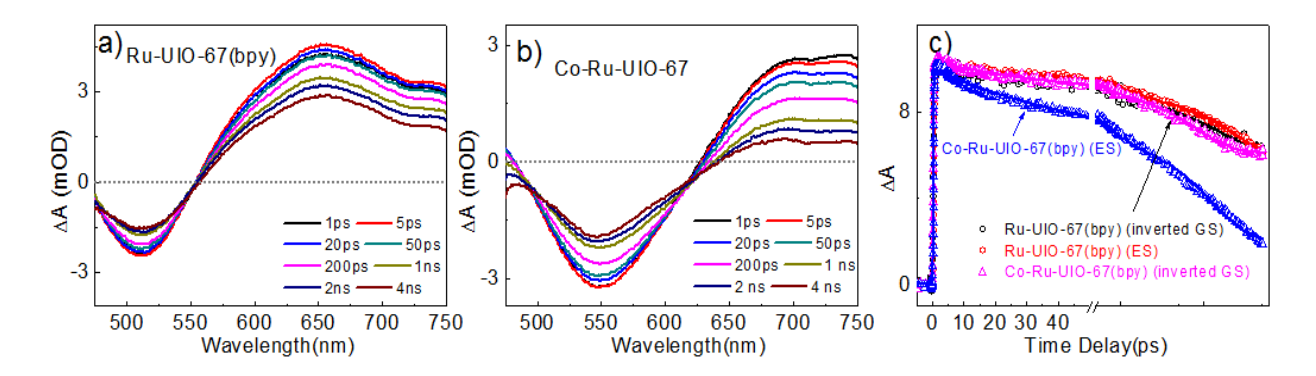


Figure 4. Femtosecond TA spectra of Ru-UIO-67(bpy) (a) and Co-Ru-UIO-67(bpy) (b). (c) The comparisons of the GSB recovery and ES decay kinetics between Ru-UIO-67(bpy) and Co-Ru-UIO-67(bpy). The GSB recovery kinetics for both Ru-UIO-67(bpy) and Co-Ru-UIO-67(bpy) were inverted in for better comparison.

Transient absorption (TA) spectroscopy was used to investigate the excited state (ES) and CS dynamics of the Co-Ru-UIO-67(bpy) MOFs. Figure 4a and 4b show the femtosecond TA spectra of Ru-UIO-67(bpy) and Co-Ru-UIO-67(bpy), respectively, following 447 nm excitation. Ru-UIO-67(bpy) was used as control sample to illustrate the intrinsic ES dynamics of Ru complex in UIO-67(bpy) framework without the presence of Co catalyst species. The TA spectra of Ru-UIO-67(bpy) show two main spectral features, i.e. a negative band centered at 513 nm and a broad absorption band at >560 nm, which can be attributed to the ground state bleach (GSB) and ES absorption of Ru complex, respectively. GSB recovery follows the same kinetics as ES decay (Figure 4c), together with the presence of an isosbestic point at 556 nm, suggesting that decay of ES molecules to their GS is the only recombination process. The TA spectra of Co-Ru-UIO-

67(bpy) (Figure 4b) also show a GSB band and a broad ES band. However, the center of the GSB band in the spectra of Co-Ru-UIO-67(bpy) shows a prominent blue shift with respect to that of Ru-UIO-67(bpy). This blue shift cannot result from the direct excitation of Co complex as negligible TA features were observed in the TA spectra of Co-UIO-67(bpy) following excitation under the same conditions. Instead, we attributed this blue shift to the formation of CS state between Ru- and Co-moieties, which was not only based on the literature reports with similar spectral shifts observed in many donor-acceptor systems,⁵⁷ but also based on our experimental observations discussed below.

As shown in Figure 4c, while the kinetics of GSB recovery and ES decay is similar in the TA spectra of Ru-UIO-67(bpy), ES kinetics decays much faster than the ESB recovery in the spectra of Co-Ru-UIO-67(bpy). Moreover, while the GSB kinetics in Co-Ru-UIO-67(bpy) remains similar as that in Ru-UIO-67(bpy), the ES kinetics is much faster in the former than the latter (Figure 4c). These results, similar to the typical features accounting for ET process from Ru complex to electron donors reported previously,⁵⁸ suggest that ET process occurs from Ru complex to Co complex in Co-Ru-UIO-67(bpy). The kinetics traces for ES decay and GSB recovery of Ru-UIO-67(bpy) as well as the GSB recovery of Co-Ru-UIO-67(bpy) can be fit by the same three-exponential decay function with fitting parameters listed in Table S3. The ES decay of Co-Ru-UIO-67(bpy) can also be fit by a three-exponential decay function (Table S3). Unfortunately, we are not able to accurately determine the ET time from the fitting results because of the presence of a long-lived decay component (>> 5 ns) which is beyond our TA time window. Nevertheless, we can conclude that ET process is much faster than the charge recombination process, as can be seen from Figure 4b where the ES decays much faster than the inverted GSB of Ru complex in Co-Ru-UIO-67(bpy).

Furthermore, the Stern-Volmer experiment (Figure S6) indicates that reductive quenching of Ru-UIO-67(bpy) by TOEA occurs on a microsecond timescale (~ 5 μs), which is much slower than ET process from Ru complex to Co complex in Co-Ru-UIO-67(bpy). Following the scheme in Figure 3c, we believe that the oxidative quenching cycle is preferred after photoexcitation of

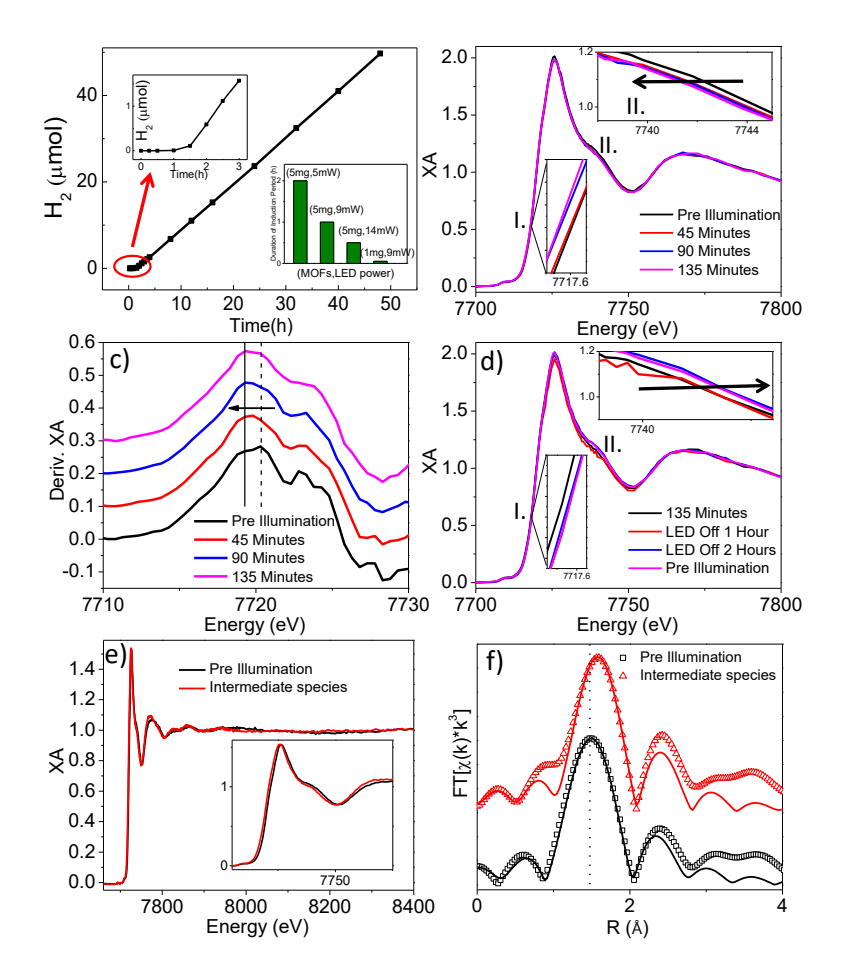


Figure 5. (a) Time profile of H₂ production by Co-Ru-UIO-67(bpy) under 447 nm LED illumination at 9 mW in the presence of TEOA (0.3 mL) and H₂O (0.4 mL) in acetonitrile solution (3 mL). The inset is the duration of induction period as a function of Co-Ru-UIO-67(bpy) concentration and LED power. (b) *In situ* XANES spectra of Co-Ru-UIO-67(bpy) as a function of irradiation times. The insets are enlarged regions I. and II. (c) The offset first derivative of *in situ* XANES spectra. (d) *In situ* XANES spectra of Co-Ru-UIO-67(bpy) after LED was switched off to observe change back to original spectrum. The comparison of XANES (e), EXAFS (inset of e), and EXAFS spectra in R space (f) of Co-Ru-UIO-67(bpy) before illumination and the intermediate species formed after induction period ends.

Co-Ru-UIO-67(bpy) under catalysis conditions.

While the CS process above is certainly the first step that initiates the photocatalytic reaction, the complete catalytic cycle includes more critical steps that lead to ultimate H₂ generation. As shown in Figure 3c, following the CS process, the catalytic pathway includes three more steps including two protonation and one reduction processes. It is essential to identify the transient species involved in these processes in order to fully understand the catalytic mechanism. In this context, *in situ* XAS, a powerful tool that can directly reveal the oxidation state and structural change of Co catalysts, was used to measure the intermediate species under the standard catalytic conditions.

In situ XAS at Co K-edge were collected at beamline 12-BM at Advanced Photon Source, Argonne National laboratory. The experiments were performed in a custom designed Teflon cell equipped with Kapton front window for X-ray irradiation and quartz rear window for LED lamp illumination and 5 mg Co-Ru-UIO-67(bpy) was used in the in-situ experiment to obtain an appropriate level of XAS signal in fluorescence mode. Under these conditions, an induction period (~ 2 hours) was observed before the production of H₂ (Figure 5a). The induction period can only be observed under certain conditions; as shown in Figure 5a (inset), the induction period is strongly dependent on LED power and MOF concentration, where high LED power and low MOF concentration decrease the duration of induction period until it cannot be resolved at the optimized condition (1 mg MOFs, 9 mW LED power). Nevertheless, the long induction period under current conditions is beneficial for unravelling the catalytic mechanism using XAS.

Figure 5b shows the *in situ* XANES spectra of Co-Ru-UIO-67(bpy) to track the change of oxidation state and structure at Co center during HER photocatalysis. Notable changes were observed in two regions of the spectrum, i.e. enlarged inset region I (edge feature) and region II

(above-edge oscillations), where both features gradually shift to lower energy during catalysis. The edge shift to lower energy was further confirmed by comparing the first derivative spectra (Figure 5c), which can be attributed to the reduction of Co^{II} to Co^I during catalysis. The shift in above-edge oscillations (region II) to lower energy are indicative of lengthening in Co-L distances where L is any coordinating atom. This structural change is likely associated with the reduction of Co center since larger degree of charge density on Co results in decreasing electrostatic attraction between Co center and ligand species, thus causing the larger bond distances observed.

It is interesting to note that the change of XANES spectrum stops after ~ 2 hours, consistent with the time frame of induction period, suggesting that the structural change observed above is associated with the induction period. These results also suggest that the induction period must be related to a chemical change that occurs in the early portion of photocatalysis, namely the formation of some intermediate chemical species that must build-up before catalysis turnover occurs. Meanwhile, upon LED illumination, the original orange solution changes to a dark grey color (Figure S7), which occurs gradually until induction period ends and occurs immediately in the system when induction period is not observed, suggesting that the color change of the MOF particles is also correlated with the induction period. Upon turning off LED light, the solution color can slowly return to its original color, which is accompanied by the returning of XANES spectra to its original state (Figure 5d). These results together suggest that the intermediate species accumulated after induction period is the active species for photocatalytic reaction rather than permanent degradation of the sample.

In order to uncover the nature of this intermediate species, we collected the *in situ* EXAFS spectra of the system after the induction period ends. As shown in Figure 5e, the whole spectrum

of the intermediate species moves to lower energy compared to the spectrum before illumination, consistent with the above in situ XANES results, suggesting that the intermediate species is Co(I) state with elongated Co-L distance. The enlarged Co-L bond distance was further confirmed by the Fourier-transformed XAFS spectrum (Figure 5f), where the peak representing the first shell (Co-N) distance is shifted to larger distance during photocatalysis, in agreement with XANES observations. To quantitatively analyze the structure of the intermediate species, FEFF with the same model utilized in section 3.1 was used to fit the EXAFS spectrum. The resulting fitting parameters are listed in Table S4. It is noted that the pre-illumination parameters show a significantly shorter distance compared to the powder Co-Ru-UIO-67(bpy) sample as well as a lower solvent coordination number, although this result is unsurprising since the local structure of Co is sensitive to solvent environment as discussed in section 3.1. Compared to the structure before illumination, the parameters of the intermediate species show significant increase in Co-N (1.98 Å increases to 2.11 Å) and Co-Cl (2.25 Å increases to 2.28 Å) distances in the first shell and increased Co-C distances in the second shell, in agreement with qualitative observation of R-space spectra. Additionally, it was observed that the solvent coordination number increased from 0.38 to 2.37 during catalysis, which we interpret as most Co atoms being uncoordinated before catalysis and most Co atoms being coordinated by two additional atoms during catalysis, considering the uncertainty in coordination number during the fit (ca. \pm 0.5 atoms). The change in coordination number could be due to multiple scenarios such as the coordination of solvent molecules to Co^I, coordination of TEOA to Co^I, or coordination of byproducts to any remaining Co^{II} in addition to Co^I. As such, we cannot definitively assign this change. However, due to the long stability of the catalysis system and the results of ex situ EXAFS fitting, we can conclude that this coordination is a dynamic event during catalysis in

solution and does not interfere with catalysis activity or permanently change the local structure of the catalytic Co center. Following the scheme presented in Figure 3c, the only possible intermediate species based on *in situ* experiments is Co^I, suggesting that the consumption of Co^I via protonation is likely the rate-determining step in HER photocatalysis. As a result, a long-lived Co^I species would certainly benefit HER reaction, which reasonably explains the observed super-high H₂ generation efficiency, as efficient CS process, i.e. ultrafast ET with inhibited charge recombination, occurs from Ru PS to Co catalyst in our Co-Ru-UIO-67(bpy) system.

In summary, we report a new robust, cost-effective single-site MOF photocatalyst by incorporation of Co active center and Ru-based photosensitizer moiety into the framework. This hybrid MOF not only exhibits exceptional hydrogen evolution activity from H₂O/acetonitrile solution but also demonstrate recyclability for at least 15 hours. Using the combination of advanced ultrafast absorption spectroscopy and *in situ* XAS, we not only captured the active intermediate species for catalysis, i.e. Co^I species formed after ET process from Ru PS to Co catalyst in MOF, but also uncovered that the consumption of this active species is the rate limiting step in photocatalysis. We thus conclude that the long-lived Co^I species due to efficient CS process is essential for efficient H₂ generation. This is likely the direct result of the heterogeneous nature of MOFs, which not only enhance the durability of the incorporated PS and molecular catalyst significantly, but also serve as versatile platform for efficient coupling of these functional components, enabling efficient solar-to-fuel conversion.

ASSOCIATED CONTENT

Supporting Information. The details of computational model, FEFF fitting, N₂ adsorption and SEM image of UIO-67(bpy), EXAFS spectra of Co-UIO-67(bpy), optimization of HER reaction,

Stern-Volmer plot, and pictures of color change during catalysis, can be found in the supporting information.

AUTHOR INFORMATION

Corresponding Author

*Jier Huang (jier.huang@marquette.edu)

Notes

The authors declare no competing financial interests.

ACKNOWLEDGMENT

This work was supported by National Science Foundation (DMR-1654140). Use of the Advanced Photon Source and nanosecond transient absorption spectroscopy at the Center for Nanoscale Materials in Argonne National Laboratory was supported by the U. S. Department of Energy, Office of Science, Office of Basic Energy Sciences, under Award No. DE-AC02-06CH11357. We thank the help from Xin Zhang and Dr. Jian Zhang in University of Nebraska-Lincoln for BET measurements.

REFERENCES

- 1. Esswein, A. J.; Nocera, D. G., Hydrogen production by molecular photocatalysis. *Chem. Rev.* **2007**, *107* (10), 4022-4047.
- 2. Lewis, N. S.; Nocera, D. G., Powering the planet: Chemical challenges in solar energy utilization. *Proc. Nat. Acad. Sci. USA* **2006**, *103* (43), 15729-15735.
- 3. Moore, G. F.; Brudvig, G. W., Energy conversion in photosynthesis: a paradigm for solar fuel production. *Annu. Rev. Condens. Matter. Phys.* **2011**, *2*, 303-327.
- 4. Reece, S. Y.; Hamel, J. A.; Sung, K.; Jarvi, T. D.; Esswein, A. J.; Pijpers, J. J. H.; Nocera, D. G., Wireless solar water splitting using silicon-based semiconductors and earth-abundant catalysts. *Science* **2011**, *334* (6056), 645-648.
- 5. Youngblood, W. J.; Lee, S. H.; Kobayashi, Y.; Hernandez-Pagan, E. A.; Hoertz, P. G.; Moore, T. A.; Moore, A. L.; Gust, D.; Mallouk, T. E., Photoassisted overall water splitting in a

- visible light-absorbing dye-sensitized photoelectrochemical cell. J. Am. Chem. Soc. 2009, 131 (3), 926-7.
- 6. McNamara, W. R.; Han, Z. J.; Alperin, P. J.; Brennessel, W. W.; Holland, P. L.; Eisenberg, R., A Cobalt-Dithiolene Complex for the Photocatalytic and Electrocatalytic Reduction of Protons. *J. Am. Chem. Soc.* **2011**, *133* (39), 15368-15371.
- 7. Gartner, F.; Sundararaju, B.; Surkus, A. E.; Boddien, A.; Loges, B.; Junge, H.; Dixneuf, P. H.; Beller, M., Light-Driven Hydrogen Generation: Efficient Iron-Based Water Reduction Catalysts. *Angew. Chem., Int. Ed.* **2009**, *48* (52), 9962-9965.
- 8. Na, Y.; Wang, M.; Pan, J. X.; Zhang, P.; Akermark, B.; Sun, L. C., Visible light-driven electron transfer and hydrogen generation catalyzed by bioinspired [2Fe2S] complexes. *Inorg. Chem.* **2008**, *47* (7), 2805-2810.
- 9. Lazarides, T.; McCormick, T.; Du, P. W.; Luo, G. G.; Lindley, B.; Eisenberg, R., Making hydrogen from water using a homogeneous system without noble metals. *J. Am. Chem. Soc.* **2009**, *131* (26), 9192-4.
- 10. Dempsey, J. L.; Brunschwig, B. S.; Winkler, J. R.; Gray, H. B., Hydrogen evolution catalyzed by cobaloximes. *Acc. Chem. Res.* **2009**, *42* (12), 1995-2004.
- 11. Yan, H. J.; Yang, J. H.; Ma, G. J.; Wu, G. P.; Zong, X.; Lei, Z. B.; Shi, J. Y.; Li, C., Visible-light-driven hydrogen production with extremely high quantum efficiency on Pt-PdS/CdS photocatalyst. *J. Catal.* **2009**, *266* (2), 165-168.
- 12. Amirav, L.; Alivisatos, A. P., Photocatalytic Hydrogen Production with Tunable Nanorod Heterostructures. *J. Phys. Chem. Lett.* **2010**, *I* (7), 1051-1054.
- 13. Acharya, K. P.; Khnayzer, R. S.; O'Connor, T.; Diederich, G.; Kirsanova, M.; Klinkova, A.; Roth, D.; Kinder, E.; Imboden, M.; Zamkov, M., The Role of Hole Localization in Sacrificial Hydrogen Production by Semiconductor-Metal Heterostructured Nanocrystals. *Nano Lett.* **2011**, *11* (7), 2919-2926.
- 14. Furukawa, H.; Cordova, K. E.; O'Keeffe, M.; Yaghi, O. M., The Chemistry and Applications of Metal-Organic Frameworks. *Science* **2013**, *341* (6149), 1230444.
- 15. Yaghi, O. M.; O'Keeffe, M.; Ockwig, N. W.; Chae, H. K.; Eddaoudi, M.; Kim, J., Reticular synthesis and the design of new materials. *Nature* **2003**, *423* (6941), 705-714.
- 16. Llabrés i Xamena, F. X.; Corma, A.; Garcia, H., Applications for metal-organic frameworks (MOFs) as quantum dot semiconductors. *J. Phys. Chem. C* **2007**, *111* (1), 80-85.
- 17. Feng, D.; Gu, Z. Y.; Li, J. R.; Jiang, H. L.; Wei, Z.; Zhou, H. C., Zirconium-metalloporphyrin PCN-222: mesoporous metal-organic frameworks with ultrahigh stability as biomimetic catalysts. *Angew. Chem.* **2012**, *51* (41), 10307-10.
- 18. Bai, Y.; Dou, Y.; Xie, L. H.; Rutledge, W.; Li, J. R.; Zhou, H. C., Zr-based metal-organic frameworks: design, synthesis, structure, and applications. *Chem. Soc. Rev.* **2016**, *45* (8), 2327-67.
- 19. Li, Z.; Xiao, J. D.; Jiang, H. L., Encapsulating a Co(II) Molecular Photocatalyst in Metal-Organic Framework for Visible-Light-Driven H-2 Production: Boosting Catalytic Efficiency via Spatial Charge Separation. *ACS Catal.* **2016**, *6* (8), 5359-5365.
- 20. Chambers, M. B.; Wang, X.; Elgrishi, N.; Hendon, C. H.; Walsh, A.; Bonnefoy, J.; Canivet, J.; Quadrelli, E. A.; Farrusseng, D.; Mellot-Draznieks, C. et al. Photocatalytic Carbon Dioxide Reduction with Rhodium-based Catalysts in Solution and Heterogenized within Metal-Organic Frameworks. *Chemsuschem* **2015**, *8* (4), 603-608.

- 21. Zhang, T.; Manna, K.; Lin, W. B., Metal-Organic Frameworks Stabilize Solution-Inaccessible Cobalt Catalysts for Highly Efficient Broad-Scope Organic Transformations. *J. Am. Chem. Soc.* **2016**, *138* (9), 3241-3249.
- 22. Rimoldi, M.; Nakamura, A.; Vermeulen, N. A.; Henkelis, J. J.; Blackburn, A. K.; Hupp, J. T.; Stoddart, J. F.; Farha, O. K., A metal-organic framework immobilised iridium pincer complex. *Chem. Sci.* **2016**, *7* (8), 4980-4984.
- 23. Kim, D.; Whang, D. R.; Park, S. Y., Self-healing of molecular catalyst and photosensitizer on metal-organic framework: robust molecular system for photocatalytic H₂ evolution from water. *J. Am. Chem. Soc.* **2016**, *138* (28), 8698-701.
- 24. de Miguel, M.; Ragon, F.; Devic, T.; Serre, C.; Horcajada, P.; Garcia, H., Evidence of photoinduced charge separation in the metal-organic framework MIL-125(Ti)-NH₂. *Chemphyschem* **2012**, *13* (16), 3651-4.
- 25. Laurier, K. G.; Fron, E.; Atienzar, P.; Kennes, K.; Garcia, H.; Van der Auweraer, M.; De Vos, D. E.; Hofkens, J.; Roeffaers, M. B., Delayed electron-hole pair recombination in iron(III)-oxo metal-organic frameworks. *PCCP* **2014**, *16* (11), 5044-7.
- 26. Fateeva, A.; Chater, P. A.; Ireland, C. P.; Tahir, A. A.; Khimyak, Y. Z.; Wiper, P. V.; Darwent, J. R.; Rosseinsky, M. J., A water-stable porphyrin-based metal-organic framework active for visible-light photocatalysis. *Angew. Chem. Int. Ed.* **2012**, *51* (30), 7440-4.
- 27. Takaishi, S.; DeMarco, E. J.; Pellin, M. J.; Farha, O. K.; Hupp, J. T., Solvent-assisted linker exchange (SALE) and post-assembly metallation in porphyrinic metal-organic framework materials. *Chem. Sci.* **2013**, *4* (4), 1509-1513.
- 28. Barron, P. M.; Wray, C. A.; Hu, C. H.; Guo, Z. Y.; Choe, W., A Bioinspired Synthetic Approach for Building Metal-Organic Frameworks with Accessible Metal Centers. *Inorg. Chem.* **2010,** *49* (22), 10217-10219.
- 29. Lee, C. Y.; Farha, O. K.; Hong, B. J.; Sarjeant, A. A.; Nguyen, S. T.; Hupp, J. T., Light-Harvesting Metal-Organic Frameworks (MOFs): Efficient Strut-to-Strut Energy Transfer in Bodipy and Porphyrin-Based MOFs. *J. Am. Chem. Soc.* **2011**, *133* (40), 15858-15861.
- 30. Xu, H. Q.; Hu, J. H.; Wang, D. K.; Li, Z. H.; Zhang, Q.; Luo, Y.; Yu, S. H.; Jiang, H. L., Visible-Light Photoreduction of CO2 in a Metal-Organic Framework: Boosting Electron-Hole Separation via Electron Trap States. *J. Am. Chem. Soc.* **2015**, *137* (42), 13440-13443.
- 31. Kent, C. A.; Mehl, B. P.; Ma, L. Q.; Papanikolas, J. M.; Meyer, T. J.; Lin, W. B., Energy Transfer Dynamics in Metal-Organic Frameworks. *J. Am. Chem. Soc.* **2010**, *132* (37), 12767-12769.
- 32. Maza, W. A.; Padilla, R.; Morris, A. J., Concentration Dependent Dimensionality of Resonance Energy Transfer in a Postsynthetically Doped Morphologically Homologous Analogue of UiO-67 MOF with a Ruthenium(II) Polypyridyl Complex. *J. Am. Chem. Soc.* **2015**, *137* (25), 8161-8168.
- 33. Zhang, S. Q.; Li, L. N.; Zhao, S. G.; Sun, Z. H.; Luo, J. H., Construction of Interpenetrated Ruthenium Metal-Organic Frameworks as Stable Photocatalysts for CO2 Reduction. *Inorg. Chem.* **2015**, *54* (17), 8375-8379.
- 34. Hou, C. C.; Li, T. T.; Cao, S.; Chen, Y.; Fu, W. F., Incorporation of a [Ru(dcbpy)(bpy)(2)](2+) photosensitizer and a Pt(dcbpy)Cl-2 catalyst into metal-organic frameworks for photocatalytic hydrogen evolution from aqueous solution. *J. Mater. Chem. A* **2015**, *3* (19), 10386-10394.
- 35. Nguyen, H. G. T.; Schweitzer, N. M.; Chang, C.-Y.; Drake, T. L.; So, M. C.; Stair, P. C.; Farha, O. K.; Hupp, J. T.; Nguyen, S. T., Vanadium-Node-Functionalized UiO-66: A Thermally

- Stable MOF-Supported Catalyst for the Gas-Phase Oxidative Dehydrogenation of Cyclohexene. *ACS Catal.* **2014**, *4* (8), 2496-2500.
- 36. Kataoka, Y.; Sato, K.; Miyazaki, Y.; Masuda, K.; Tanaka, H.; Naito, S.; Mori, W., Photocatalytic hydrogen production from water using porous material [Ru-2(p-BDC)(2)](n). *Energ. Environ. Sci.* **2009**, *2* (4), 397-400.
- 37. Wang, C.; Xie, Z. G.; deKrafft, K. E.; Lin, W. L., Doping Metal-Organic Frameworks for Water Oxidation, Carbon Dioxide Reduction, and Organic Photocatalysis. *J. Am. Chem. Soc.* **2011**, *133* (34), 13445-13454.
- 38. Huang, R. Y.; Peng, Y.; Wang, C.; Shi, Z.; Lin, W. B., A Rhenium-Functionalized Metal-Organic Framework as a Single-Site Catalyst for Photochemical Reduction of Carbon Dioxide. *Eur. J. Inorg. Chem.* **2016**, (27), 4358-4362.
- 39. Nasalevich, M. A.; Becker, R.; Ramos-Fernandez, E. V.; Castellanos, S.; Veber, S. L.; Fedin, M. V.; Kapteijn, F.; Reek, J. N. H.; van der Vlugt, J. I.; Gascon, J., Co@NH₂-MIL-125(Ti): cobaloxime-derived metal-organic framework-based composite for light-driven H₂ production. *Energ. Environ. Sci.* **2015**, 8 (1), 364-375.
- 40. Sasan, K.; Lin, Q. P.; Mao, C. Y.; Feng, P. Y., Incorporation of iron hydrogenase active sites into a highly stable metal-organic framework for photocatalytic hydrogen generation. *Chem. Commun.* **2014**, *50* (72), 10390-10393.
- 41. Pullen, S.; Fei, H. H.; Orthaber, A.; Cohen, S. M.; Ott, S., Enhanced Photochemical Hydrogen Production by a Molecular Diiron Catalyst Incorporated into a Metal-Organic Framework. *J. Am. Chem. Soc.* **2013**, *135* (45), 16997-17003.
- 42. Sawano, T.; Lin, Z. K.; Boures, D.; An, B.; Wang, C.; Lin, W. B., Metal-Organic Frameworks Stabilize Mono(phosphine)-Metal Complexes for Broad-Scope Catalytic Reactions. *J. Am. Chem. Soc.* **2016**, *138* (31), 9783-9786.
- 43. Kim, D.; Whang, D. R.; Park, S. Y., Self-Healing of Molecular Catalyst and Photosensitizer on Metal-Organic Framework: Robust Molecular System for Photocatalytic H-2 Evolution from Water. *J. Am. Chem. Soc.* **2016**, *138* (28), 8698-8701.
- 44. Zhou, T. H.; Du, Y. H.; Borgna, A.; Hong, J. D.; Wang, Y. B.; Han, J. Y.; Zhang, W.; Xu, R., Postc-synthesis modification of a metalc-organic framework to construct a bifunctional photocatalyst for hydrogen production. *Energ. Environ. Sci.* **2013**, *6* (11), 3229-3234.
- 45. Burgess, S. A.; Kassie, A.; Baranowski, S. A.; Fritzsching, K. J.; Schmidt-Rohr, K.; Brown, C. M.; Wade, C. R., Improved Catalytic Activity and Stability of a Palladium Pincer Complex by Incorporation into a Metal–Organic Framework. *J. Am. Chem. Soc.* **2016**, *138* (6), 1780-1783.
- 46. Fei, H. H.; Cohen, S. M., A robust, catalytic metal-organic framework with open 2,2 'bipyridine sites. *Chem. Commun.* **2014**, *50* (37), 4810-4812.
- 47. Yu, X.; Cohen, S. M., Photocatalytic metal-organic frameworks for the aerobic oxidation of arylboronic acids. *Chem. Commun.* **2015**, *51* (48), 9880-9883.
- 48. Xie, P. H.; Hou, Y. J.; Zhang, B. W.; Cao, Y.; Wu, F.; Tian, W. J.; Shen, J. C., Spectroscopic and electrochemical properties of ruthenium(II) polypyridyl complexes. *J. Chem. Soc., Dalton Trans.* **1999**, (23), 4217-4221.
- 49. Katz, M. J.; Brown, Z. J.; Colon, Y. J.; Siu, P. W.; Scheidt, K. A.; Snurr, R. Q.; Hupp, J. T.; Farha, O. K., A facile synthesis of UiO-66, UiO-67 and their derivatives. *Chem. Commun.* **2013**, *49* (82), 9449-9451.

- 50. Nickerl, G.; Leistner, M.; Helten, S.; Bon, V.; Senkovska, I.; Kaskel, S., Integration of accessible secondary metal sites into MOFs for H2S removal. *Inorg. Chem. Front.* **2014**, *1* (4), 325-330.
- 51. Pattengale, B.; Yang, S. Z.; Ludwig, J.; Huang, Z. Q.; Zhang, X. Y.; Huang, J., Exceptionally Long-Lived Charge Separated State in Zeolitic Imidazolate Framework: Implication for Photocatalytic Applications. *J. Am. Chem. Soc.* **2016**, *138* (26), 8072-8075.
- 52. Galoisy, L.; Cormier, L.; Calas, G.; Briois, V., Environment of Ni, Co and Zn in low alkali borate glasses: information from EXAFS and XANES spectra. *J. Non-Cryst. Solids* **2001**, 293, 105-111.
- 53. Wu, Z. Y.; Xian, D. C.; Hu, T. D.; Xie, Y. N.; Tao, Y.; Natoli, C. R.; Paris, E.; Marcelli, A., Quadrupolar transitions and medium-range-order effects in metal K-edge x-ray absorption spectra of 3d transition-metal compounds. *Phys. Rev. B* **2004**, *70* (3), 033104
- 54. Gonzalez, M. I.; Bloch, E. D.; Mason, J. A.; Teat, S. J.; Long, J. R., Single-Crystal-to-Single-Crystal Metalation of a Metal-Organic Framework: A Route toward Structurally Well-Defined Catalysts. *Inorg. Chem.* **2015**, *54* (6), 2995-3005.
- 55. Ravel, B.; Newville, M., ATHENA, ARTEMIS, HEPHAESTUS: data analysis for X-ray absorption spectroscopy using IFEFFIT. *J. Synchrotron Radiat* **2005**, *12* (4), 537-541.
- 56. Kim, D.; Whang, D. R.; Park, S. Y., Self-Healing of Molecular Catalyst and Photosensitizer on Metal-Organic Framework: Robust Molecular System for Photocatalytic H₂ Evolution from Water. *J. Am. Chem. Soc.* **2016**, *138* (28), 8698-8701.
- 57. Bairu, S. G.; Mghanga, E.; Hasan, J.; Kola, S.; Rao, V. J.; Bhanuprakash, K.; Giribabu, L.; Wiederrecht, G. P.; da Silva, R.; Rego, L. G. C. et al. Ultrafast Interfacial Charge-Transfer Dynamics in a Donor-pi-Acceptor Chromophore Sensitized TiO₂ Nanocomposite. *J. Phys. Chem. C* **2013**, *117* (9), 4824-4835.
- 58. Taira, N.; Saitoh, M.; Hashimoto, S.; Moon, H. R.; Yoon, K. B., Effect of electron-acceptor strength of zeolite on the luminescence decay rate of Ru(bpy)₃²⁺ incorporated within zeolites. *Photoch. Photobio. Sci.* **2006**, *5* (9), 822-827.